Disclaimer

The findings and conclusions in this report are those of the authors and do not necessarily represent the views of the Ministry of Health, Labour and Welfare, Japan.

References

[1] Donaldson K, Poland CA. Nanotoxicology: new insights into nanotubes. Nature nanotechnology. 2009; 4: 708-10.

[2] Kohyama N, Suzuki Y. Analysis of asbestos fibers in lung parenchyma, pleural plaques, and mesothelioma tissues of North American insulation workers. Ann N Y Acad Sci. 1991; 643: 27-52.

[3] Donaldson K, Poland CA, Murphy FA, MacFarlane M, Chernova T, Schinwald A. Pulmonary toxicity of carbon nanotubes and asbestos - similarities and differences. Advanced drug delivery reviews. 2013; 65: 2078-86.

[4] Takagi A, Hirose A, Nishimura T, et al. Induction of mesothelioma in p53+/- mouse by intraperitoneal application of multi-wall carbon nanotube. The Journal of toxicological sciences. 2008; 33: 105-16.

[5] Sakamoto Y, Nakae D, Fukumori N, et al. Induction of mesothelioma by a single intrascrotal administration of multi-wall carbon nanotube in intact male Fischer 344 rats. The Journal of toxicological sciences. 2009; 34: 65-76.

[6] Nagai H, Okazaki Y, Chew SH, et al. Diameter and rigidity of multiwalled carbon nanotubes are critical factors in mesothelial injury and carcinogenesis. Proc Natl Acad Sci U S A. 2011; 108: E1330-8.

[7] Takagi A, Hirose A, Futakuchi M, Tsuda H, Kanno J. Dose-dependent mesothelioma induction by intraperitoneal administration of multi-wall carbon nanotubes in p53 heterozygous mice. Cancer science. 2012; 103: 1440-4.

[8] Donaldson K, Murphy FA, Duffin R, Poland CA. Asbestos, carbon nanotubes and the pleural mesothelium: a review of the hypothesis regarding the role of long fibre retention in the parietal pleura, inflammation and mesothelioma. Particle and fibre toxicology. 2010; 7: 5.

[9] Mercer RR, Hubbs AF, Scabilloni JF, et al. Distribution and persistence of pleural penetrations by multi-walled carbon nanotubes. Particle and fibre toxicology. 2010; 7: 28.

[10] Porter DW, Hubbs AF, Mercer RR, et al. Mouse pulmonary dose- and time course-responses induced by exposure to multi-walled carbon nanotubes. Toxicology. 2010; 269: 136-47.

[11] Xu J, Futakuchi M, Shimizu H, et al. Multi-walled carbon nanotubes translocate into the pleural cavity and induce visceral mesothelial proliferation in rats. Cancer science. 2012; 103: 2045-50.

[12] Mercer RR, Scabilloni JF, Hubbs AF, et al. Extrapulmonary transport of MWCNT following inhalation exposure. Particle and fibre toxicology. 2013; 10: 38.

[13] Murphy FA, Poland CA, Duffin R, Donaldson K. Length-dependent pleural inflammation and parietal pleural responses after deposition of carbon nanotubes in the pulmonary airspaces of mice. Nanotoxicology. 2013; 7: 1157-67.

[14] Porter DW, Hubbs AF, Chen BT, et al. Acute pulmonary dose-responses to inhaled multi-walled carbon nanotubes. Nanotoxicology. 2013; 7: 1179-94.

[15] Kasai T, Umeda Y, Ohnishi M, et al. Thirteen-week study of toxicity of fiber-like multi-walled carbon nanotubes with whole-body inhalation exposure in rats. Nanotoxicology. 2014: 1-10.

[16] Xu J, Alexander DB, Futakuchi M, et al. Size- and shape-dependent pleural translocation, deposition, fibrogenesis, and mesothelial proliferation by multiwalled carbon nanotubes. Cancer science. 2014; 105: 763-9.

[17] Ryman-Rasmussen JP, Cesta MF, Brody AR, et al. Inhaled carbon nanotubes reach the subpleural tissue in mice. Nature nanotechnology. 2009; 4: 747-51.

[18] Li ZF, Luo GH, Wei F, Xiang R, Liu YP. The quantitative characterization of the concentration and dispersion of multi-walled carbon nanotubes in suspension by spectrophotometry. Nanotechnology. 2006; 17: 3692-8.

[19] Xu J, Futakuchi M, Iigo M, et al. Involvement of macrophage inflammatory protein 1alpha (MIP1alpha) in promotion of rat lung and mammary carcinogenic activity of nanoscale titanium dioxide particles administered by intra-pulmonary spraying. Carcinogenesis. 2010; 31: 927-35.

[20] Xu J, Futakuchi M, Alexander DB, et al. Nanosized zinc oxide particles do not promote DHPN-induced lung carcinogenesis but cause reversible epithelial hyperplasia of terminal bronchioles. Archives of toxicology. 2014; 88: 65-75.

[21] Numano T, Xu J, Futakuchi M, et al. Comparative study of toxic effects of anatase and rutile type nanosized titanium dioxide particles in vivo and in vitro. Asian Pacific journal of cancer prevention : APJCP. 2014; 15: 929-35.

[22] Ohnishi M, Yajima H, Kasai T, et al. Novel method using hybrid markers: development of an approach for pulmonary measurement of multi-walled carbon nanotubes. Journal of occupational medicine and toxicology. 2013; 8: 30.

[23] Blackshear PE, Pandiri AR, Ton TV, et al. Spontaneous mesotheliomas in F344/N rats are characterized by dysregulation of cellular growth and immune function pathways. Toxicol Pathol. 2014; 42: 863-76.

[24] Ma-Hock L, Treumann S, Strauss V, et al. Inhalation toxicity of multiwall carbon nanotubes in rats exposed for 3 months. Toxicological sciences : an official journal of the Society of Toxicology. 2009; 112: 468-81.

[25] Mercer RR, Scabilloni JF, Hubbs AF, et al. Distribution and fibrotic response following inhalation exposure to multi-walled carbon nanotubes. Particle and fibre toxicology. 2013; 10: 33.

[26] Pauluhn J. Subchronic 13-week inhalation exposure of rats to multiwalled carbon nanotubes: toxic effects are determined by density of agglomerate structures, not fibrillar structures. Toxicological sciences : an official journal of the Society of Toxicology. 2010; 113: 226-42.

[27] Yu KN, Kim JE, Seo HW, Chae C, Cho MH. Differential toxic responses between pristine and functionalized multiwall nanotubes involve induction of autophagy accumulation in murine lung. Journal of toxicology and environmental health Part A. 2013; 76: 1282-92.

[28] Sargent LM, Porter DW, Staska LM, et al. Promotion of lung adenocarcinoma following inhalation exposure to multi-walled carbon nanotubes. Particle and fibre toxicology. 2014; 11: 3.

[29] Stone KC, Mercer RR, Gehr P, Stockstill B, Crapo JD. Allometric relationships of cell numbers and size in the mammalian lung. American journal of respiratory cell and molecular biology. 1992; 6: 235-43.

[30] Galer DM, Leung HW, Sussman RG, Trzos RJ. Scientific and practical considerations for the development of occupational exposure limits (OELs) for chemical substances. Regulatory toxicology and pharmacology : RTP. 1992; 15: 291-306.

[31] Bates DV, Fish BR, Hatch TF, Mercer TT, Morrow PE. Deposition and retention models for internal dosimetry of the human respiratory tract. Task group on lung dynamics. Health Phys. 1966; 12: 173-207.

[32] EPA/600/P-99/002bF. Air Quality Criteria for Particulate Matter. Volume II. 2004.

[33] Liou SH, Tsai CS, Pelclova D, Schubauer-Berigan MK, Schulte PA. Assessing the first wave of epidemiological studies of nanomaterial workers. J Nanopart Res. 2015; 17: 413.

[34] Fatkhutdinova LM, Khaliullin TO, Shvedova AA. Carbon Nanotubes Exposure Risk Assessment: From Toxicology to Epidemiologic Studies (Overview of the Current Problem). Nanotechnol Russ. 2015; 10: 501-9.

[35] Aiso S, Kubota H, Umeda Y, et al. Translocation of intratracheally instilled multiwall carbon nanotubes to lung-associated lymph nodes in rats. Industrial health. 2011; 49: 215-20.

[36] Sargent LM, Reynolds SH, Castranova V. Potential pulmonary effects of engineered carbon nanotubes: in vitro genotoxic effects. Nanotoxicology. 2010; 4: 396-408.

[37] Murphy FA, Poland CA, Duffin R, et al. Length-dependent retention of carbon nanotubes in the pleural space of mice initiates sustained inflammation and progressive fibrosis on the parietal pleura. The American journal of pathology. 2011; 178: 2587-600.

[38] Costa R, Orriols R. Man-made mineral fibers and the respiratory tract. Arch Bronconeumol. 2012; 48: 460-8.

[39] Colotta F, Allavena P, Sica A, Garlanda C, Mantovani A. Cancer-related inflammation, the seventh hallmark of cancer: links to genetic instability. Carcinogenesis. 2009; 30: 1073-81.

[40] Coussens LM, Werb Z. Inflammation and cancer. Nature. 2002; 420: 860-7.

[41] Crusz SM, Balkwill FR. Inflammation and cancer: advances and new agents. Nat Rev Clin Oncol. 2015; 12: 584-96.

[42] Lu H, Ouyang W, Huang C. Inflammation, a key event in cancer development. Mol Cancer Res. 2006; 4: 221-33.

[43] Barna BP, Huizar I, Malur A, et al. Carbon nanotube-induced pulmonary granulomatous disease: Twist1 and alveolar macrophage M1 activation. Int J Mol Sci. 2013; 14: 23858-71.

[44] Meng J, Li X, Wang C, Guo H, Liu J, Xu H. Carbon nanotubes activate macrophages into a M1/M2 mixed status: recruiting naive macrophages and supporting angiogenesis. ACS Appl Mater Interfaces. 2015; 7: 3180-8.

[45] Murphy FA, Schinwald A, Poland CA, Donaldson K. The mechanism of pleural inflammation by long carbon nanotubes: interaction of long fibres with macrophages stimulates them to amplify pro-inflammatory responses in mesothelial cells. Particle and fibre toxicology. 2012; 9: 8.

[46] Aldieri E, Fenoglio I, Cesano F, et al. The role of iron impurities in the toxic effects exerted by short multiwalled carbon nanotubes (MWCNT) in murine alveolar macrophages. Journal of toxicology and environmental health Part A. 2013; 76: 1056-71.

[47] Fenoglio I, Tomatis M, Lison D, et al. Reactivity of carbon nanotubes: free radical generation or scavenging activity? Free radical biology & medicine. 2006; 40: 1227-33.

[48] Wang Y, Okazaki Y, Shi L, et al. Role of hemoglobin and transferrin in multi-wall carbon nanotube-induced mesothelial injury and carcinogenesis. Cancer science. 2016; 107: 250-7.

Figure legends

Figure 1

Before administration, a portion of the MWCNT-N suspension was fractionated by passing it through a sieve with a pore size of 35 μm. SEM images of MWCNT-N in the (A) Unfiltered preparation, (B) Flow-Through fraction, and (C) Retained fraction are shown. The mean length of the unfiltered MWCNT-N in the administration dispersant was 4.2±2.9 μm and that of the MWCNT-N in the flow-through fraction was 2.6±1.6 μm. The size of the MWCNT-N retained by the filtering sieve could not be measured because of the dense agglomerates the retained fibers formed due to the loss of the PF68 dispersant during fractionation.

Figure 2

Accumulation of MWCNT-N in the lung (A and B) and lymph node (C and D). MWCNT-N was found in the lung alveoli either in the granulation tissue or macrophages. (A) MWCNT-N shows granular and needle like shapes. Aggregations of MWCNT-phagocytosed macrophages can be seen (arrow). The inset shows a polarizing lens image of the aggregation of MWCNT-phagocytosed macrophages; arrows point to the same macrophage aggregation in the main panel and the inset. MWCNT-N aggregates that cause polarization can clearly be seen in the inset. Granular agglomerations of MWCNT-N do not cause polarization. (B) MWCNT-N also caused thick fibrotic granulation tissue formation (arrow) and calcification (*). The inset shows a polarizing lens image of granulation tissue with deposition of MWCNT-N. Arrows point to the same lesion in the main panel and the inset. (C) Accumulation of MWCNT-N in the mediastinal lymph node. The inset shows a polarizing lens image. Arrows point to the same MWCNT-N accumulations in the main panel and the inset. (D) Accumulation of MWCNT-N in periaortic connective tissue showing fibrotic thickening. The inset shows a polarizing lens image. (E) MWCNT-N is present in the periphery of the malignant mesothelioma tissue.

Figure 3

Kaplan Meier survival plot of the rats in the Untreated, Vehicle Control, Unfiltered MWCNT , Flow-Through MWCNT fraction, and Retained MWCNT fraction groups.

Figure 4

Malignant mesotheliomas in the pleural/mediastinal cavity. Malignant mesothelioma showing invasion of the pericarpdium (A), myocardium (B), periesopahgeal tissue (C) and visceral pleura(D)

Figure 5

Malignant mesothelioma, sarcomatoid type, in the pleural cavity. (A) Tumor cells arranged in a solid manner and form spherical . Immunostaining of Calretinin (B), Wilms tumor protein (WT-1) (C), Podoplanin (Pod) (D), and Thyroid transcription facter-1 (TTF-1) (E). In the high power magnification images (inset), the cytoplasm of the tumor cells were faintly stained by Cal and WT-1. The nuclei is also faintly stained by Pod. Cytoplasm and nuclei are entirely unstained by TTF-1.

Figure 6

Bronchiolar epithelium of 109 week old untreated rat. Haematoxylin and Eosin staining (H&E) (A) and Cal (B), WT-1 (C), Pod (D), and TTF-1 (E) staining. The cytoplasm is slightly stained by Cal and WT-1. Nuclei are clearly positive for TTF-1.

Figure 7

Gross appearance of lung adenocarcinoma in the pericardial pleural cavity. Histologically, the tumor is composed of packed small epithelial-like cells forming incomplete glandular structures (see Figure 11A) with invasion of pericardial and diaphragm tissues (arrows). The tumor was positive for TTF-1. Small tumor nodules of the same histological appearance were found in the lung (circle).

Figure 8

Lung bronchiolo-alveolar adenoma (adenoma). H&E (A), Cal (B), WT-1 (C), Pod (D), and TTF-1 (E) staining. The cytoplasm is slightly stained by Cal and WT-1. Nuclei are clearly positive for TTF-1.

Figure 9

Bronchiolo-alveolar carcinoma (adenocarcinoma) of the lung. H&E (A), Cal (B), WT-1 (C), Pod (D), and TTF-1 (E) staining. The cytoplasm is slightly stained by Cal and WT-1. Nuclei are clearly positive for TTF-1.

Figure 10

Adenocarcinoma of the lung forming a large mass in the pleural cavity with invasion of the heart and diaphragm and remote metastasis to the kidney. H&E (A), Cal (B), WT-1 (C), Pod (D) and

TTF-1 (E) staining. The cytoplasm is slightly stained by Cal and WT-1. Nuclei are clearly positive in TTF-1.

Figure 11

Adenocarcinoma of the lung forming a large mass in the pleural cavity with invasion of the paribronchial lymphnodes, serosal pericardium, and diaphragm (see Figure 3). Densely proliferating small tumor cells with round nuclei are arranged in an incomplete glandular or solid manner. H&E (A), Cal (B), WT-1 (C), Pod (D) and TTF-1 (E) staining. The cytoplasm is slightly stained by WT-1. All the nuclei are clearly positive in TTF-1 indicating lung alveolar cell origin. After histological examination, this case was initially diagnosed as an epithelial mesothelioma; however, after staining with TTF-1, the tumor was re-diagnosed as a lung adenocarcinoma.

Table 1. Size of MWCNT-N in the preparation medium and in the lung tissue

	MWCNT-N in the preparation medium before administration	MWCNT-N in the lung tissue	
MWCNT-N Fraction		Alveolar Wall	Tumor area
Unfiltered	4.2 ± 2.9[a]	3.1 ± 1.0	2.0 ± 0.4
Flow-through	2.6 ± 1.6	2.8 ± 0.9	2.6 ± 0.6
Retained	> 2.6	3.2 ± 0.8	3.2 ± 0.7

[a]Mean ± SD μm

Table 2. Amount of MWCNT-N in the lung at weeks 2 and 109

Week 2			Week 109			
Rats[a]	MWCNT-N Fraction	Amount[b]	Rats[a]	MWCNT-N Fraction	Amount[b]	Ratio of week 109 to week 2
5	Unfiltered	605 ± 119	5	Unfiltered	486 ± 44	80%
4	Flow-through	603 ± 238	4	Flow-through	426 ± 116	71%
5	Retained	701 ± 176	5	Retained	268 ± 43	38%

[a] Number of rats examined

[b] μg MWCNT-N per gram wet-weight paraformaldehyde fixed lung tissue

Table 3. Incidence of pleural malignant mesothelioma and lung tumors

MWCNT Fraction	Rats	Malignant Mesothelioma	Lung Tumors			Total Tumor burden (%)
		Pericardial and/or Pleura (%)	Adenoma	Adeno-carcinoma	Combined (%)	
NT	15	0 (0.0)	0	0	0 (0.0)	0 (0.0)
V	13	0 (0.0)	0	0	0 (0.0)	0 (0.0)
NT + V	28	0 (0.0)	0	0	0 (0.0)	0 (0.0)
U	12	3[a] (25.0)	1	3[a]	4 (33.3)	7 (58.3)
FT	12	3 (25.0)	1	2	3 (25.0)	6 (50.0)
R	14	0 (0.0)	2	5	7 (50.0)	7 (50.0)
U + FT + R	38	6 (15.8)*	4	10	14 (36.8)**	20 (52.6)**

NT, No treatment; V, Vehicle; U, Unfiltered; FT, Flow-through; R, Retained

Average length: U = 4.2 ± 2.9 μm; FT = 2.6 ± 1.6 μm; R was not measurable

[a] One rat had both a malignant mesothelioma and a lung adenocarcinoma

* $p<0.05$; ** $p<0.001$ vs. the control groups (NT+V)

1

Table 4. Tumor incidence in other organs[a]

MWCNT Fraction	Rats	Abdominal cavity mesothelioma (%)	Leydig cell tumor (%)	Leukemia/ lymphoma (%)	Subcutaneous fibroma (%)	Pureputial gland tumor (%)	Pituitary gland tumor (%)
NT	15	0	10 (66.7)	0	4 (26.7)	0	0
V	13	2 (15.4)	10 (76.9)	2 (15.4)	2 (15.4)	1 (7.7)	1 (7.7)
NT + V	28	2 (7.1)	20 (71.4)	2 (7.1)	2 (7.1)	1 (3.6)	1 (3.6)
U	13	1 (7.7)	9 (69.2)	4 (30.8)	0	0	1 (7.7)
FT	13	1 (7.7)	8 (61.5)	3 (23.1)	1 (7.7)	1 (7.7)	2 (15.4)
R	15	0	8 (53.3)	3 (20.0)	1 (6.7)	0	1 (6.7)
U + FT + R	41	2 (4.9)	25 (61.0)	10 (24.4)	2 (4.9)	1 (2.4)	4 (9.8)

NT, No treatment; V, Vehicle; U, Unfiltered; FT, Flow-through; R, Retained

Average length: U = 4.2 ± 2.9 μm; FT = 2.6 ± 1.6 μm; R was not measurable

[a] Including 1 adrenal cortical adenoma in NT, 1 liver adenoma in FT and 1 sarcoma of unknown origin in R.

Table 5. Physical characteristics of MWCNT-7 and MWCNT-N

	MWCNT-7	MWCNT-N
Length	1-4 μm (38%)	1-4 μm (51%)
Length	5-20 μm (58%)	5-20 μm (47%)
Diameter	20-100 nM (98%)	30-100 nM (95%)
Layers	35 - 40	10
Iron Content	0.3 - 0.4%	0.04 - 0.05%

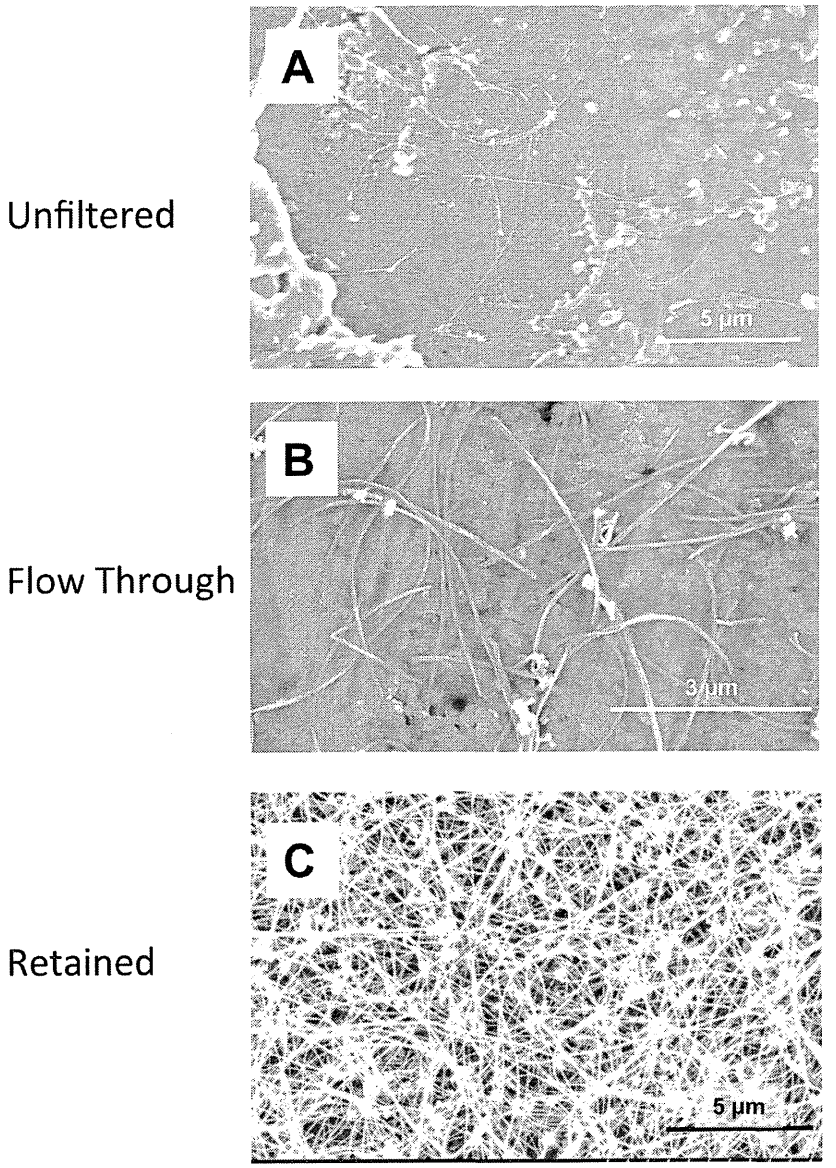

Figure 1
120x170mm (600 x 600 DPI)

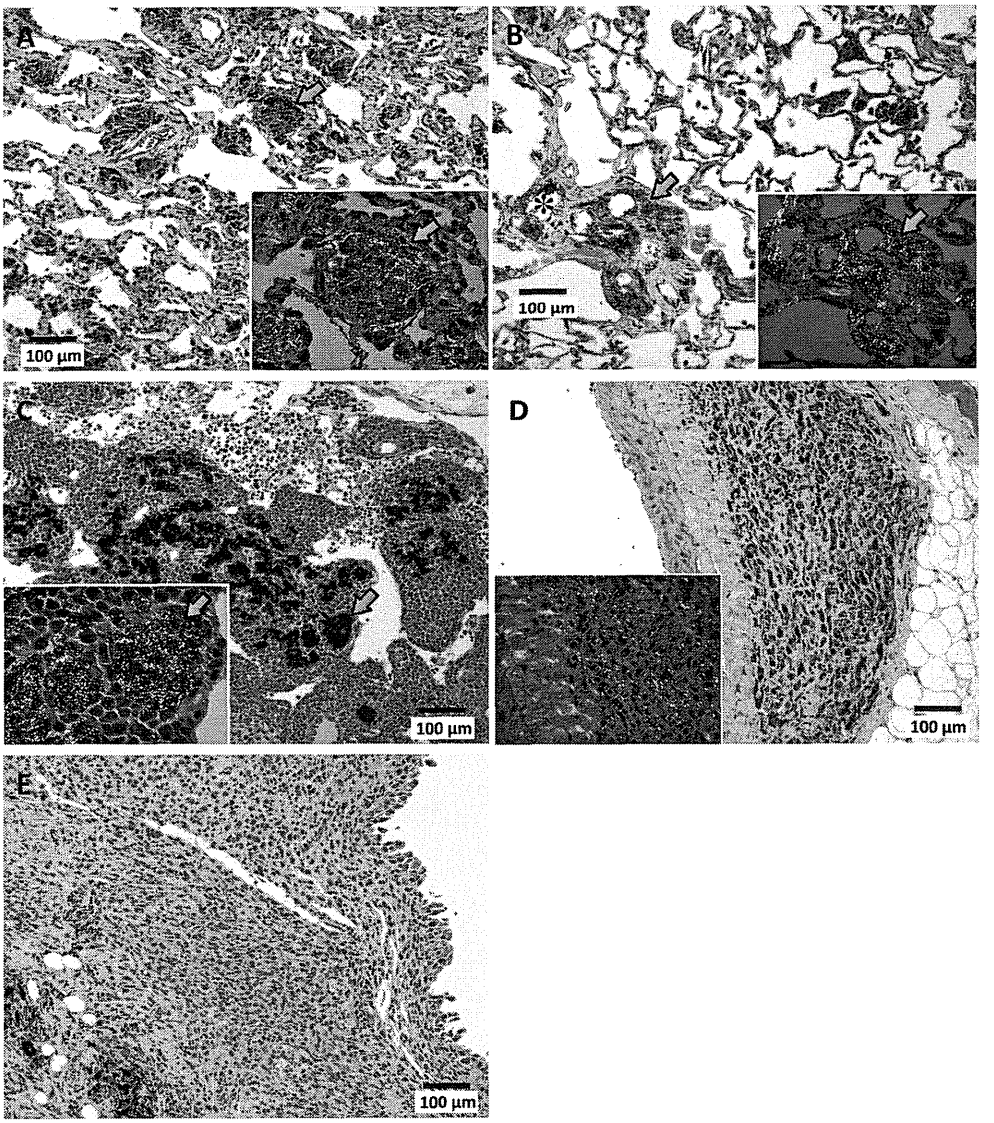

Figure 2
193x221mm (300 x 300 DPI)

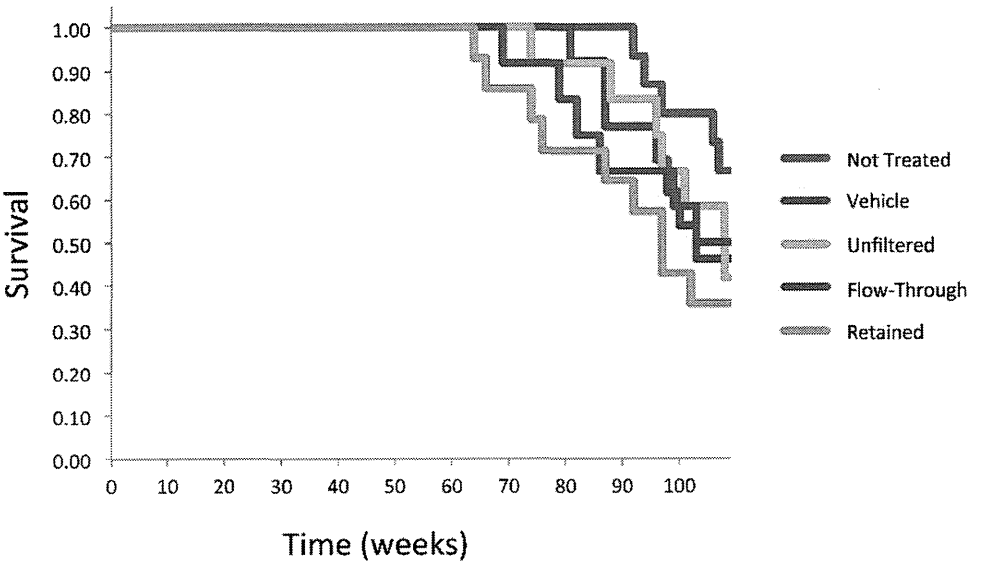

Figure 3
85x51mm (300 x 300 DPI)

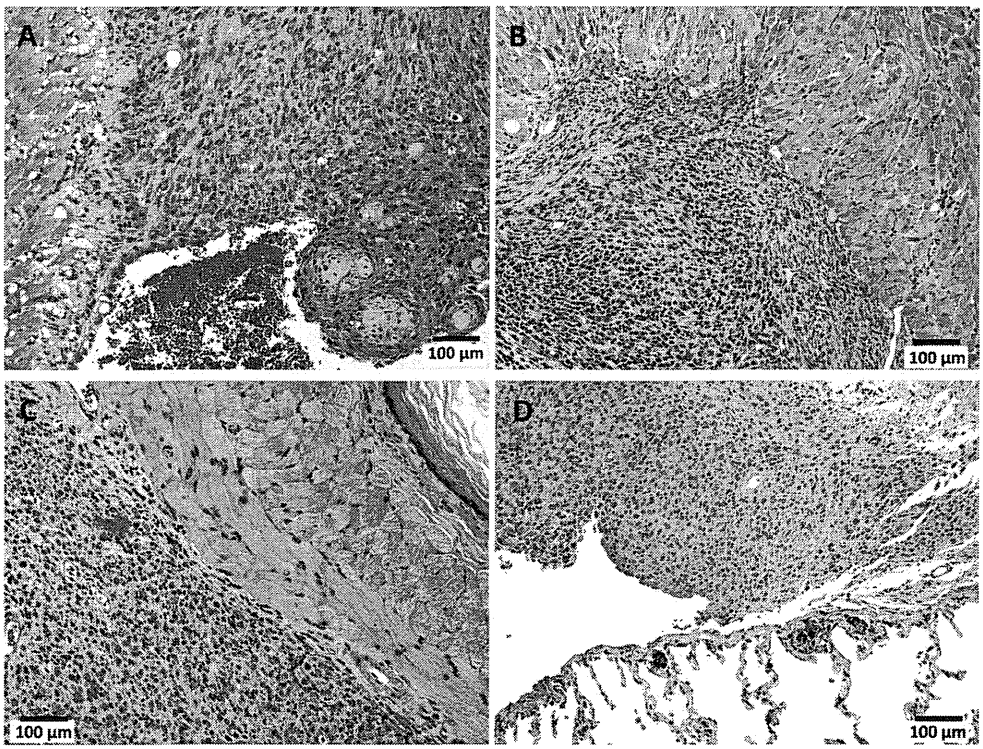

Figure 4
129x97mm (300 x 300 DPI)

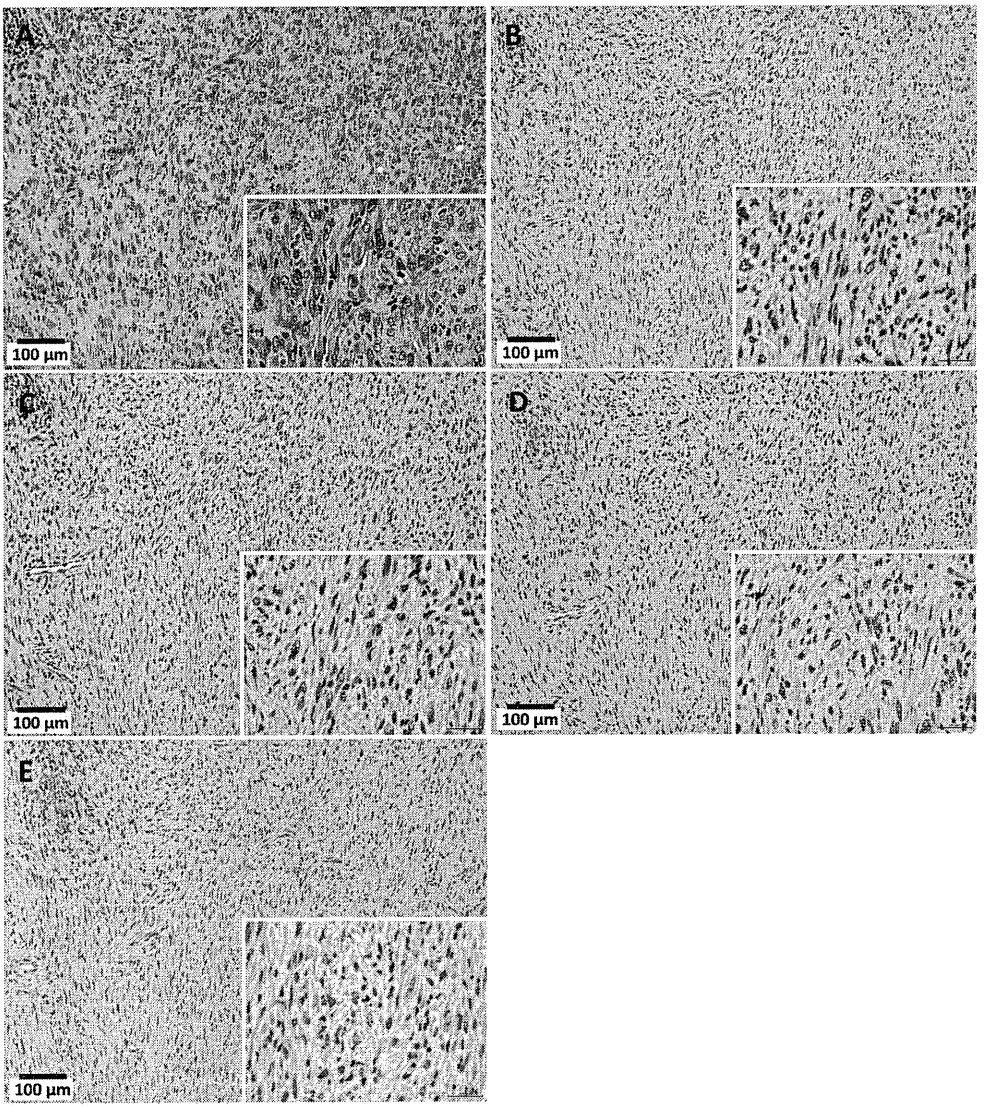

Figure 5
214x241mm (300 x 300 DPI)

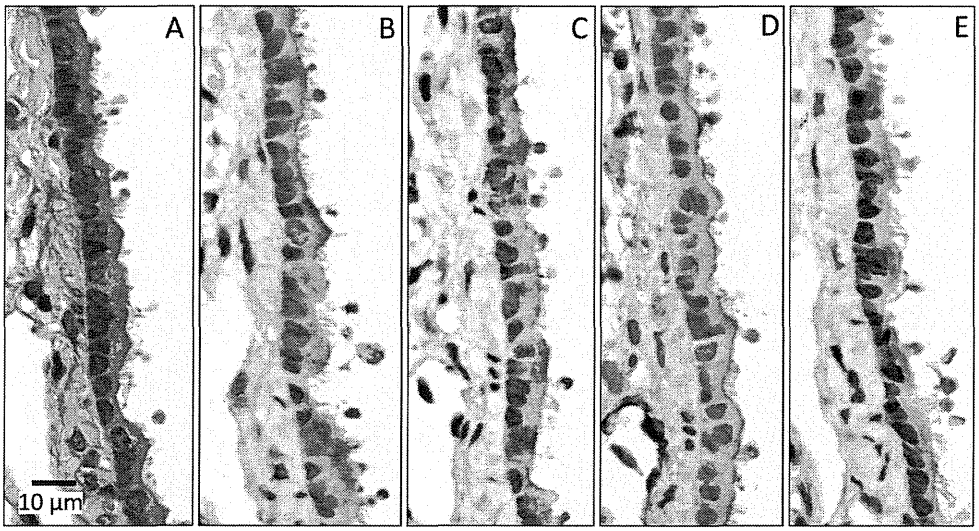

Figure 6
91x49mm (600 x 600 DPI)

Figure 7
103x126mm (600 x 600 DPI)

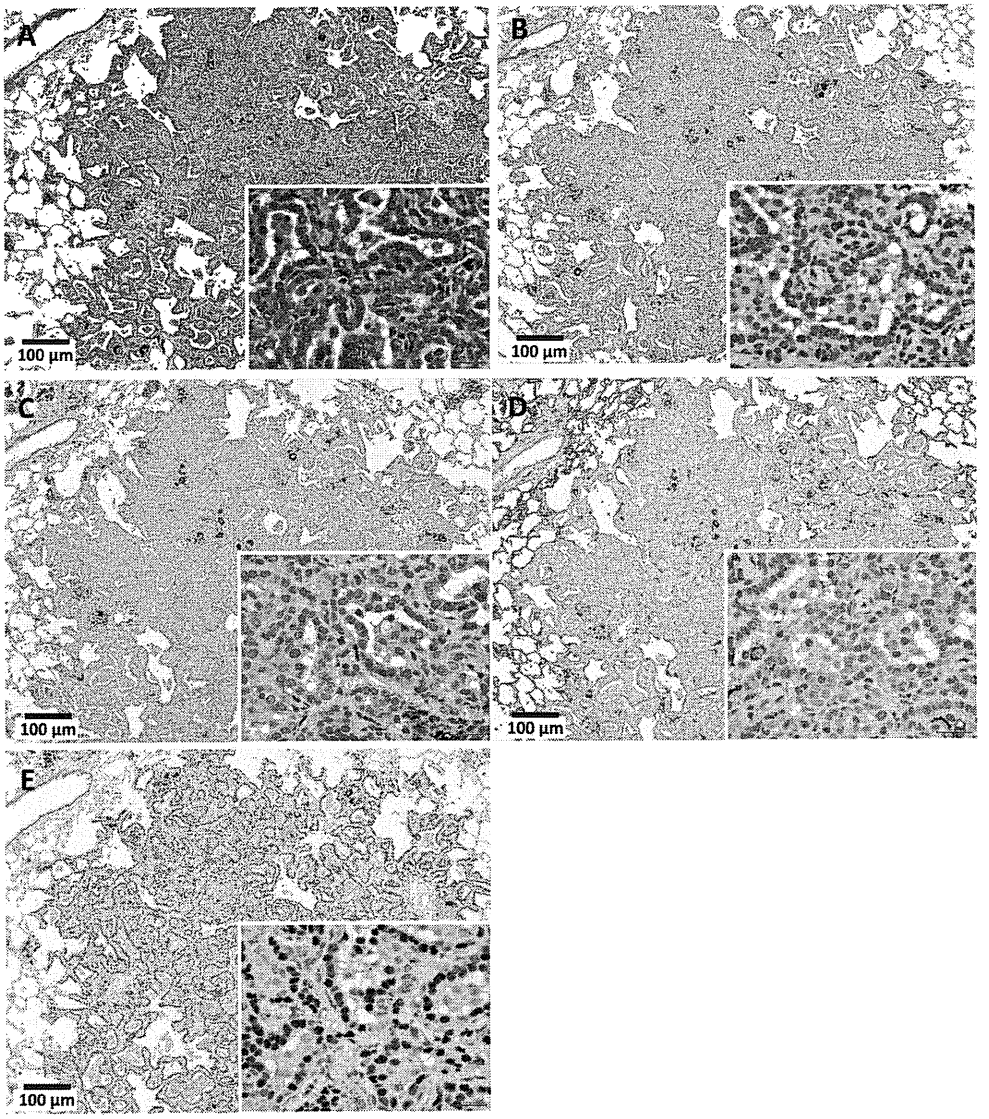

Figure 8
193x219mm (300 x 300 DPI)

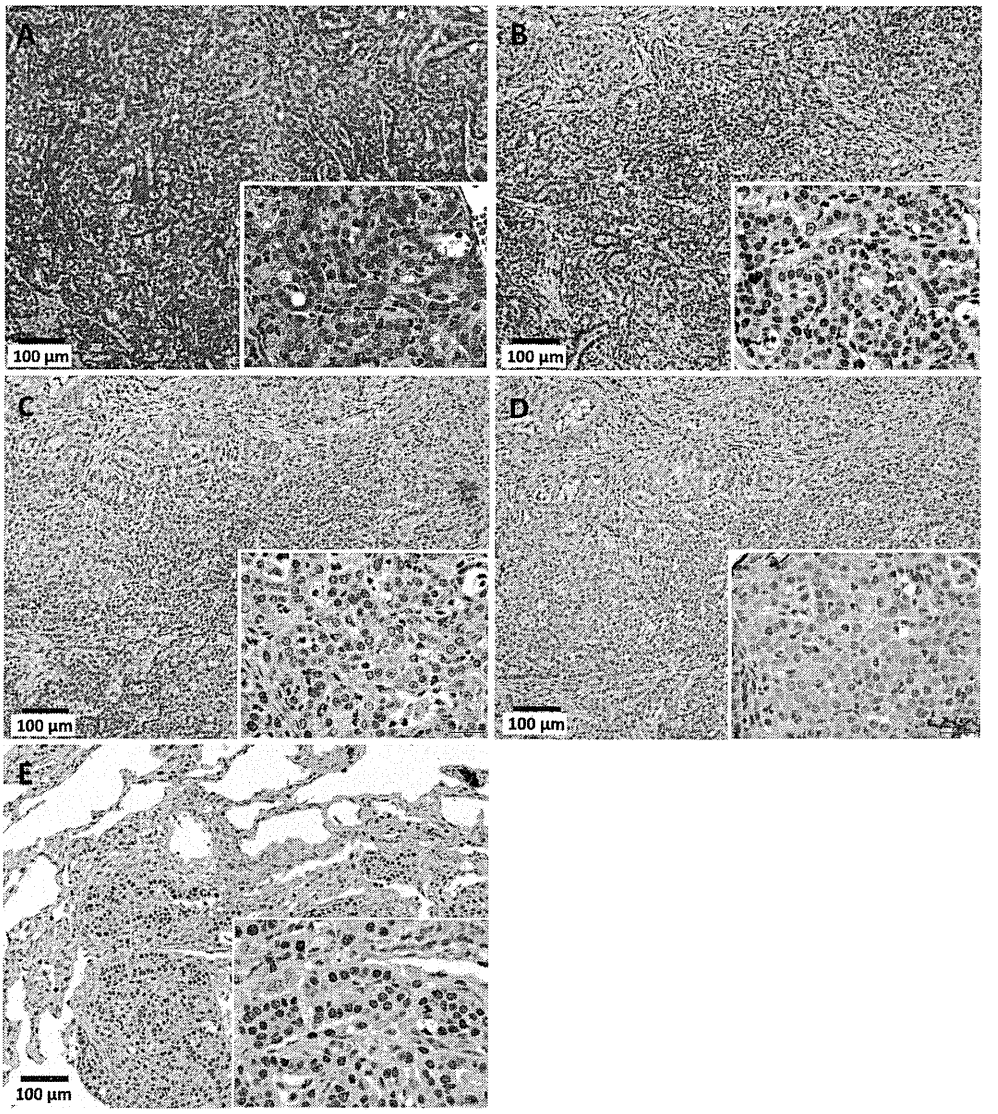

Figure 9
215x244mm (300 x 300 DPI)